

pubs.acs.org/JPCB Article

Intermolecular Hydrogen Bonding Tunes Vibronic Coupling in Heptazine Complexes

Emily J. Rabe, Harrison J. Goldwyn, Doyk Hwang, David J. Masiello, and Cody W. Schlenker*



Cite This: J. Phys. Chem. B 2020, 124, 11680-11689



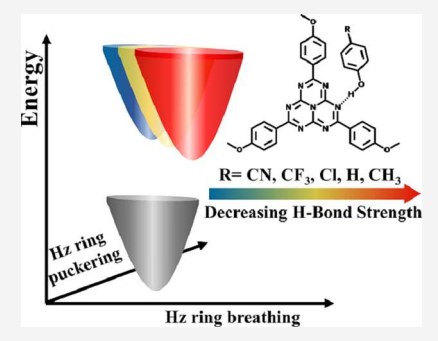
ACCESS

Metrics & More



Supporting Information

ABSTRACT: To better understand how hydrogen bonding influences the excited-state landscapes of aza-aromatic materials, we studied hydrogen-bonded complexes of 2,5,8-tris (4-methoxyphenyl)-1,3,4,6,7,9,9b-heptaazaphenalene (TAHz), a molecular photocatalyst related to graphitic carbon nitride, with a variety of phenol derivatives (R-PhOH). By varying the electron-withdrawing character of the para-substituent on the phenol, we can modulate the strength of the hydrogen bond. Using time-resolved photoluminescence, we extract a spectral component associated with the R-PhOH-TAHz hydrogen-bonded complex. Surprisingly, we noticed a striking change in the relative amplitude of vibronic peaks in the TAHz-centered emission as a function of R-group on phenol. To gain a physical understanding of these spectral changes, we employed a displaced-oscillator model of molecular emission to fit these spectra. This fit assumes that two vibrational modes are dominantly coupled to the emissive electronic transition and extracts their



frequencies and relative nuclear displacements (related to the Huang-Rhys factor). With the aid of quantum chemical calculations, we found that heptazine ring-breathing and ring-puckering modes are likely responsible for the observed vibronic progression, and both modes indicate decreasing molecular distortion in the excited state with increasing hydrogen bond strength. This finding offers new insights into intermolecular excited-state hydrogen bonding, which is a crucial step toward controlling excited-state proton-coupled electron transfer and proton transfer reactions.

■ INTRODUCTION

Excited-state proton transfer and proton-coupled electron transfer reactions, both inter- and intramolecular, are ubiquitous in biological and chemical transformations such as photosynthesis and photopolymerization. 1-6 For these reactions, understanding the interplay between electronic and vibrational motions within a hydrogen-bonded complex is critical.^{7,8} Yet, studying hydrogen bonding, especially in the excited state, is complicated, given the short lifetimes, dynamic reorganizations, and numerous photochemical branching pathways of these complexes. 9-12 This has led to ambiguity in even simple quantities such as the excited-state hydrogenbonding association constants, as the calculation requires deconvoluting the rate of excited-state hydrogen bond formation and excited-state reactivity. 13 The picture becomes further complicated by the presence of multiple hydrogenbonding sites for many heteroaromatic materials and the hydrogen-bonding networks created by high concentrations of hydrogen bond donors. 12,14 These complications must be considered in order to understand and control the reactivity of intermolecular complexes and generally map how the excitedstate landscape is influenced by hydrogen bond formation.

Past work considering intermolecular excited-state protoncoupled electron transfer (ES-PCET) reactions has demonstrated that the hydrogen bond coordinate can largely predict excited-state reactivity by calculating the energy of a charge transfer state along that hydrogen bond coordinate. ^{15–17} In this framework, we generally assume that changing the quencher (hydrogen bond donor) alters only the energy and position of the charge transfer state, which ultimately determines reaction rates. It is relatively rare to consider the chromophore's intrinsic molecular vibrations as a significant contributor to intermolecular PCET, despite the need for coordination of nuclear and electronic motion across a hydrogen bond. However, there has been a great deal of work to understand the interconnectedness of molecular vibrations and proton transfer in the context of intramolecular hydrogen bonding, particularly regarding excited-state intermolecular proton transfer reactions. 5,6,18-21 This work has shown how O-H stretching frequencies can couple to lower frequency molecular vibrations of a chromophore, which is somewhat intuitive because all the atoms are covalently linked. It is currently an open question as to what extent this insight extends to intermolecular chemical reactions and whether it is possible to manipulate reaction dynamics or pathways by vibrational excitation.

Received: August 24, 2020 Revised: November 24, 2020 Published: December 14, 2020





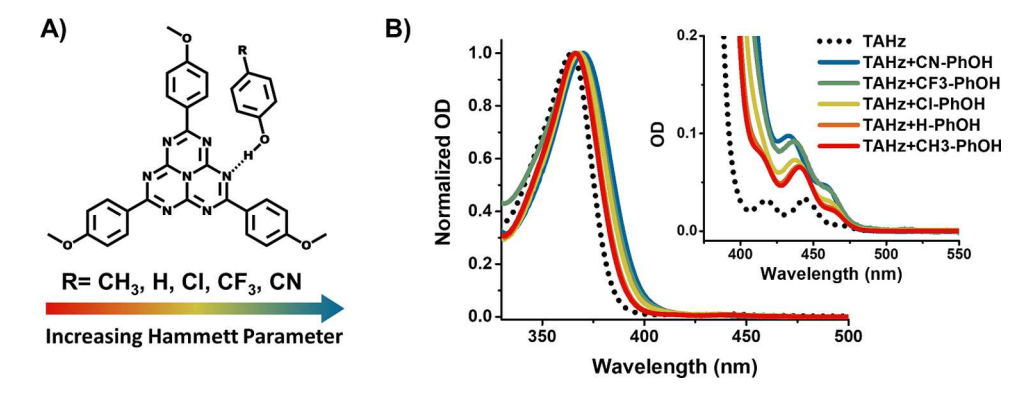


Figure 1. Para-substituted phenols serve as a model system for understanding how changing electronegativity, quantified by the Hammett parameter, changes the hydrogen bond strength with heptazine. (B) Effect of increasing the Hammett parameter can be seen in the ground-state absorption of TAHz in toluene. The bright $\pi\pi^*$ transition red-shifts with the increasing Hammett parameter. The lower-energy and weaker transitions (inset) appear to show the opposite effect: they blue shift and begin to overlap with the tail of the bright transition. All phenol concentrations were 50 mM.

If achievable, this kind of reaction control would be extremely useful in the context of poly(heptazine imides), commonly termed carbon nitride, which has become a model organic material for driving a host of intermolecular photochemical reactions. 22-26 Yet, fundamental photophysical studies aimed at understanding the ground- and excited-state hydrogen bonding of these materials are currently few, owing to the structural ambiguity in this nitrogen-rich material.^{27,2} To gain insights into the heptazine hydrogen bonding, integral to several carbon nitride-catalyzed reactions, we have chosen a model heptazine-based chromophore (TAHz), previously used to study the heptazine-driven ES-PCET reaction. 17,29,30 In previous studies, we found that the quenching rate constant of TAHz with different phenols generally followed the driving force for electron transfer.¹⁷ However, when comparing H-PhOH and Cl-PhOH, which have the same oxidation potential, we observed a faster quenching rate constant for Cl-PhOH. Barman and co-workers observed a similar effect with coumarin and attributed this to hydrogen bonding. 11 In this study, we explore how hydrogen bonding influences the excited-state energy landscape and reactivity using timeresolved photoluminescence spectroscopy (TR-PL) together with a displaced-oscillator model of molecular emission and quantum chemical calculations. We use TR-PL to extract emission spectra from hydrogen-bonded complexes of heptazine using global analysis.¹⁷ As we change the Hammett parameter of the phenol derivative, we notice a surprising change in the vibronic progression of emission from the hydrogen-bonded complexes. Analysis of the spectral lineshape provides insights beyond the strength of the hydrogen bond and allows us to understand how hydrogen bonding influences molecular distortions between the ground and excited states. Modeling the vibronic excitations as a pair of displaced harmonic oscillators captures the spectral shape of emission from these hydrogen-bonded complexes and allows us to extract both a high and low-frequency mode that are significantly coupled to the S₁ transition.³¹ From this analysis, we quantify how the displacement along representative nuclear coordinates changes as a function of the R-group on the hydrogen-bonded phenol. Using quantum chemical calculations, we further visualize representative vibrational modes to build a more holistic picture of how molecular distortions can affect ES-PCET and ES-PT reactivity.

MATERIALS AND METHODS

Reagents. Urea, potassium hydroxide, phosphorous oxychloride, phosphorous pentachloride, phenol, and 4-(trifluoromethyl)phenol were all purchased from Sigma-Aldrich. Anisole (99%) was purchased from Alfa Aesar. Aluminum chloride was purchased from Fischer Scientific. p-Cresol, 4-chlorophenol, and 4-hydroxybenzonitrile were all purchased from TCI. All reagents were used without further purification.

Synthesis. The full synthetic and characterization procedure of TAHz was the same as described in our previous publication in the Supporting Information.²⁹

Sample Preparation. TAHz was dissolved in toluene (20 μ M) and stirred overnight before measurements were performed to ensure minimal aggregation effects. Samples were kept in the dark until measurements were performed.

Ground-State Absorption. Ground-state absorption spectra were collected using a Cary5000 UV–vis–NIR spectrometer. Within each R-PhOH series, the same TAHz stock solution was used to ensure consistent TAHz concentration with the varying phenol derivatives. Each solution of the spectra shown in Figure 1 was 7.5 μ M TAHz and 50 mM R-PhOH.

For the data collected in Figure 2, the initial TAHz concentration was 7.5 μ M in toluene. Using a 3 M PhOH stock solution in toluene, 10 μ L of PhOH solution was added and stirred, and a spectrum was recorded. This process was repeated 10 times. Then, 20 μ L aliquots were added, stirred, and recorded 10 times. The resulting 21 (1 with no PhOH and 20 with sequential additions) spectra were baseline-corrected by subtracting the average OD from 495–500 nm. Each spectrum was then multiplied by the fraction TAHz was diluted by (new total volume/old volume). The PhOH concentration was calculated by accounting for the change in volume upon each addition.

TR-PL Spectra. TR-PL spectra were collected using a Hamamatsu streak camera (C10910) with a slow-sweep unit (M10913–01) in photon-counting mode. Samples were irradiated with 50 fs pulses at 365 nm and 1 kHz pump from a Coherent/Light Conversion OPerA solo optical parametric amplifier and taken on a 10 ns time range with a resolution of 20 ps and an instrument response function width of \sim 90 ps. Pump fluences were approximately 2.7 \times 10¹³ photons cm⁻². All samples for global analysis were prepared to

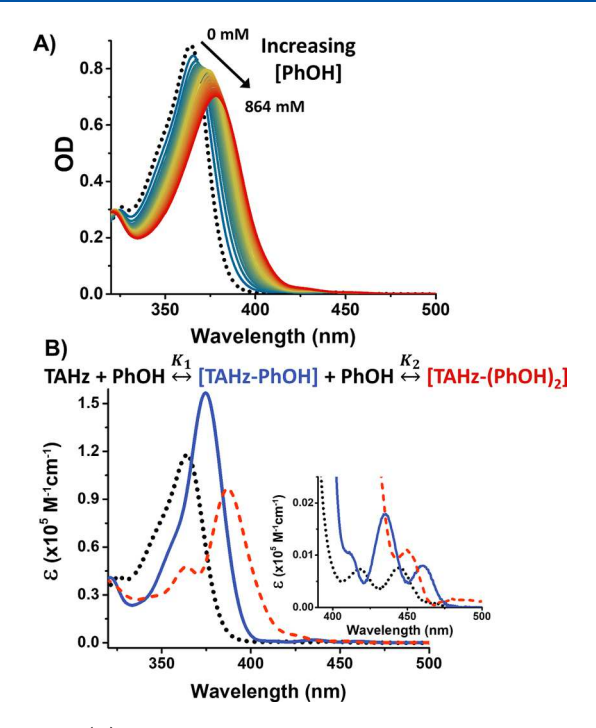


Figure 2. (A) Ground-state absorption spectra of TAHz in neat toluene (dotted back line) and upon increasing PhOH concentrations ranging from 30–860 mM (blue to red). The lack of a clear isosbestic point suggested that there are more than two absorbing species; this could be due to the existence of a second hydrogen-bonded complexation. The measurement was taken by sequential additions of a 3 M PhOH stock solution, and the resulting spectra were corrected for changing TAHz concentration. (B) Data fit well to a double-complexation model, and using an iterative least-squares method, we were able to extract the individual components and association constants $K_1 = 6.43$ M⁻¹ and $K_2 = 1.61$ M⁻¹. The extracted traces for unbound (black dotted), singly bound (blue solid), and doubly bound (dashed red) complexes show a red shift of the bright transition and blue shift of the weak transitions.

be 50 μ M TAHz and 100 mM R-PhOH, with the exception of CN-PhOH, which was 50 mM because of solubility constraints. Notably, the spectral shape of the fast component was not found to be dependent on the concentration of R-PhOH. For each R-PhOH, the solution was made and measured in duplicate. The resulting extracted duplicate spectra from global analysis were averaged together prior to fitting. No smoothing was performed on the data. Prior to fitting, the x-axis was converted to energy in eV. The y-axis was adjusted accordingly (intensity/eV = (intensity/nm) \times (1240 nm \times eV)/eV/eV), where intensity/nm was the original y-axis value. The spectra were then area-normalized.

Calculations. Density functional theory (DFT) and time-dependent DFT (TD-DFT) calculations were carried out with Gaussian16.³² The Becke 3-Parameter Lee-Yang-Parr (B3LYP) functional and 6-31G(d,p) Pople basis set were used. We first optimized ground-state geometry of the TAHz molecule and calculated normal modes and IR spectrum. The scaling factor of the vibrational wavenumber for comparison with the experimental FT-IR spectrum was 0.97. For excited-state optimized geometry, TD-DFT optimization was performed at lowest singlet excited state of TAHz (symmetry-forbidden $\pi\pi^*$ transition). For calculation of the TAHz-Cl-PhOH complex, the solvent effect was included by the polarizable continuum model (PCM) with a dielectric constant of toluene ($\varepsilon = 2.3741$) in the Gaussian16 package.

■ RESULTS AND DISCUSSION

Varying the Phenol to Increase Hydrogen Bond Strength. Substituted phenols are ubiquitous in systematic studies on PT and PCET reactions. 2,33,34 Phenols are often considered to act as "functionalized water," wherein we can change the oxidation potential and pKa of the hydroxyl group by changing a functional group on the phenyl ring. However, these two properties are often intertwined; adding an electronwithdrawing group to the phenol will likely increase its oxidation potential and decrease its pKa. Previously, we focused on the quenching rate constant as a function of oxidation potential for heptazine-phenol systems.¹⁷ In this study, we are interested in exploring the hydrogen-bonded complexes formed and understanding how the energy landscape is perturbed by changing the electronic nature of the R-group. To quantify the electron-withdrawing strength of the R-group, we will use the calculated Hammett parameter for each substituent in the para-position; values are shown in Table 1.35 These well-accepted parameters allow us to quantitatively rank a wide range of phenols, as we explore their hydrogen-bonded complexes formed with TAHz, as shown in Figure 1A.

To study the strength of the ground-state hydrogen bond, it is common to use ground-state absorption spectroscopy to monitor the free versus bound populations as a function of the concentration of the hydrogen bond donor. The absorption spectrum of TAHz, and other heptazine derivatives, comprises a series of closely spaced electronic transitions with varying oscillator strengths and is discussed in detail elsewhere. The strength is attributed to a bright intramolecular charge transfer $\pi\pi^*$ transition, and the lowest-lying transition shown in the inset of Figure 1B is attributed to the symmetry-forbidden $S_1(\pi\pi^*)$ state. To study how the strength of hydrogen bonding affects these electronic transitions, we can compare the absorption spectrum of TAHz in the presence of

Table 1. Extracted Parameters from the Displaced-Oscillator Model for Each Vibrational Mode

		mode 1		mode 2		
R	Hammett parameter $(\sigma_{ m p})^{35}$	frequency (cm ⁻¹)	HR ₁ ^a	frequency (cm ⁻¹)	HR_2	calculated H-bond length (Å)
CH ₃	-0.17	1068.92 ± 0.04	1.513	128.043 ± 0.004	3.6 ± 0.9	1.940
Н	0	1070.37 ± 0.05	1.444	185.68 ± 0.02	2.24 ± 0.02	1.937
Cl	0.227	1061.96 ± 0.04	1.372	159.12 ± 0.01	2.36 ± 0.02	1.924
CF_3	0.54	1057.08 ± 0.05	1.103	179.92 ± 0.04	1.77 ± 0.02	1.910
CN	0.66	1035.49 ± 0.02	1.034	156.800 ± 0.004	1.924 ± 0.007	1.904

 $^{^{}a}$ Uncertainty < $\pm 10^{-3}$

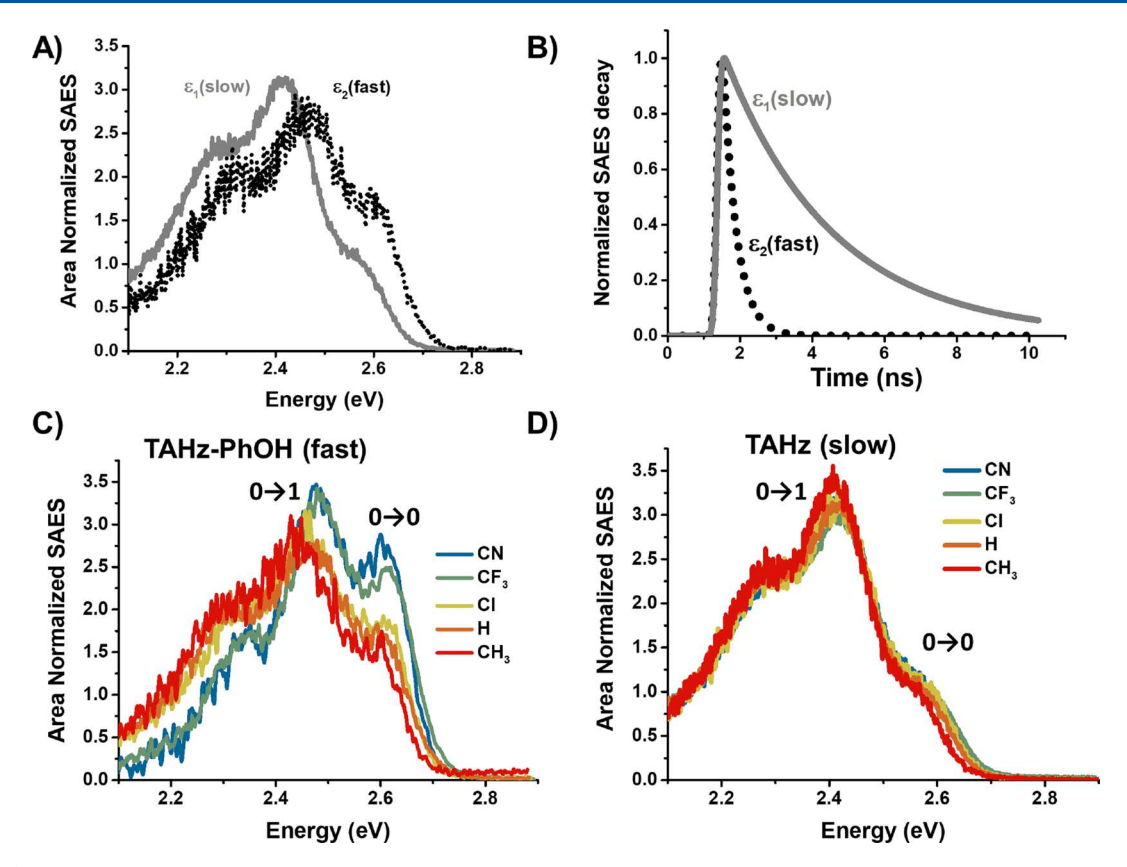


Figure 3. (A) From the TR-PL data of TAHz in toluene with 100 mM PhOH, we are able extract, using global analysis, two distinct species-associated emission spectra (SAES). (B) These species decay at different rates, one with a shorter lifetime of 0.36 ns (black dots) and one with a longer lifetime of 3.2 ns (gray solid). We attribute species decaying more slowly to unbound excited-state TAHz chromophores, whereas the fast component is attributed to an excited-state hydrogen-bonded complex. (C) We see a significant change in the spectral shape of the fast component depending on the R-group of the phenol: CN (blue), CF₃ (green), Cl (yellow), H (orange), and CH₃ (red). D) We do not observe significant spectral differences in the slow component.

different R-PhOH's. When the same concentration of each phenol is present with TAHz in toluene, we observe variations in the magnitude of peak shifts in Figure 1B. We observe that larger shifts correlate with larger Hammett parameters. As expected, this suggests that higher association constants, indicating stronger hydrogen bonds, are seen for more electron-withdrawing R-groups on the phenol species. This is supported by quantum chemical calculations of the hydrogen bond length for each TAHz-R-PhOH complex listed in Table 1 and previous $K_{\rm A}$ estimates. ¹⁷

Previously, we analyzed TAHz-R-PhOH complexes, assuming only conversion from unbound TAHz to TAHz-PhOH and estimated KA's accordingly. 17 However, heptazine-based materials, and TAHz specifically, are capable of forming multiple hydrogen bonds because of the numerous heteroatoms. Multiple hydrogen bonds can complicate the analysis, as different hydrogen-bonded complexes can have different spectral features. This is evident in the absence of a clear isosbestic point upon increasing the hydrogen bond donor concentration, as shown in Figure 2A. The spectral shape does not converge to that of a hydrogen-bonded complex; therefore, it requires deconvolution to extract the absorption spectra associated with different hydrogen-bonded complexes from concentration-dependent absorption data. Using the framework laid out by Demeter and co-workers, we are able to model the concentration-dependent absorption spectra, assuming that TAHz undergoes two distinct hydrogen-bonding events with two association constants.¹⁴ Under this assumption, we can model the total absorption at wavelength λ as the sum of three component spectra $A_{\lambda} = \epsilon_{\mathrm{T}\lambda}[T] + \epsilon_{\mathrm{TX}\lambda}[\mathrm{TX}] + \epsilon_{\mathrm{TX}\lambda}[\mathrm{TX}_2]$, where $\epsilon_{\mathrm{T}\lambda}$, $\epsilon_{\mathrm{TX}\lambda}$, and $\epsilon_{\mathrm{TX}\lambda}$ are the molar extinction coefficients of TAHz (T), a 1:1 complex of TAHz-PhOH (TX) , and a 1:2 complex of TAHz-(PhOH) $_2$ (TX_2) , respectively. We can express $[\mathrm{TX}]$ and $[\mathrm{TX}_2]$ in terms of concentration of phenol and the two association constants $(K_1$ and $K_2)$, described in detail in Section SII. By performing a least-squares fit to the absorption vs $[\mathrm{PhOH}]$ curves iteratively for each wavelength, we are able to extract the parameters $\epsilon_{\mathrm{TX}\lambda}$, $\epsilon_{\mathrm{TX},\lambda}$, K_1 , and K_2 . While TAHz could form more than two hydrogen bonds, the data in this concentration range appear to be fit well by accounting for only two distinct spectral shapes; see Figure S1.

Figure 2B compares the molar absorptivity spectrum of TAHz compared to the extracted spectra for TAHz-PhOH and TAHz-(PhOH)₂. However, despite being able to extract the absorption spectra for the TAHz-PhOH and TAHz-(PhOH)₂ complexes shown in Figure 2B, the red-shifting of the bright $\pi\pi^*$ state and the blue-shifting of the S₁ state obscure the vibronic progression for these hydrogen-bonded complexes. Therefore, while we would ideally compare the vibronic structure in both the absorption and emission spectra, we must instead rely on TR-PL measurements where we can kinetically resolve individual emission components. Additionally, using the two extracted K_A values, we can estimate the relative

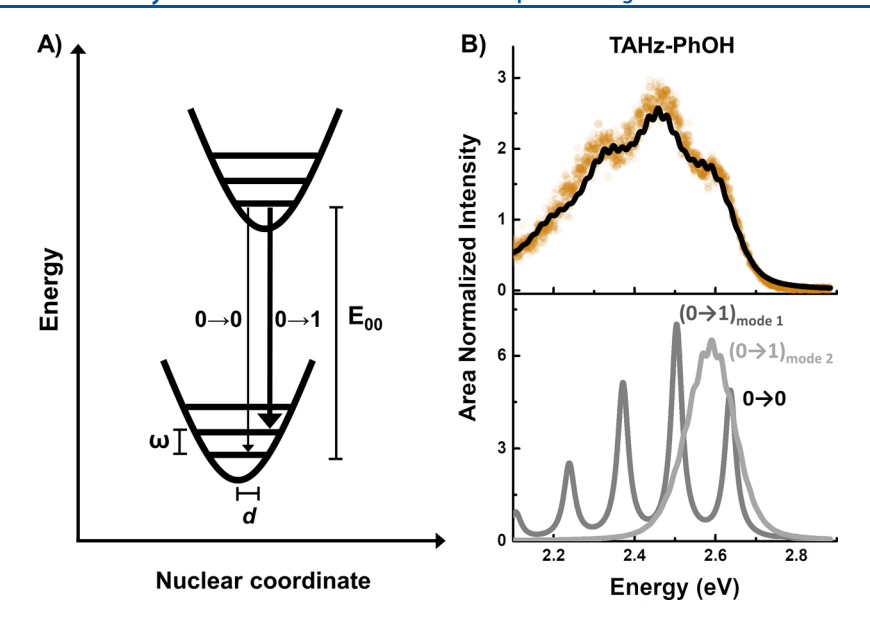


Figure 4. (A) Pictorial representation of the model parameters for one vibrational mode adiabatically coupled to the emissive electronic transition. The harmonic wells represent the vibrational potential energy surfaces in the ground and first excited electronic state separated by energy E_{00} . Each well has a series of vibrational states spaced by energy ω . The displacement of the excited-state potential equilibrium position relative to the ground state, d, represents the molecular distortion along that specific vibrational coordinate. This displacement gives rise to varying overlap between the zeroth vibrational state wave function in the electronic excited state and the vibrations in the electronic ground state well, resulting in varying probability of emission, shown by the $0 \to 0$ and $0 \to 1$ emission lines. (B) Extracted TAHz-PhOH emission (orange dots) is fit well by the model (black line), assuming that two vibrational modes are coupled to the electronic transition: one low-frequency mode around 200 cm⁻¹ and one high-frequency mode around 1050 cm⁻¹. The bottom plot shows the emission spectra from each of the two vibrational modes independently, with the low-frequency mode in light gray and the high-frequency mode in dark gray. Because both modes are coupled to the same electronic transition, the two-mode model fit (top panel) to the data is instead a convolution of the two-component curves in the bottom panel.

amounts of each complex at the time of excitation for a given phenol concentration and choose our conditions accordingly.

Time-Resolved Photoluminescence. In the absence of a hydrogen bond donor, the TAHz emission exhibits a monoexponential decay (Figure S2). When a hydrogen bond donor, such as phenol, is present, then we observe two kinetically distinct components. Keeping in mind the possibility of a 1:2 complex, we chose a low concentration of phenol (100 mM) in order to focus our study on the 1:1 complex. From the K_A values extracted above, we can calculate the concentration, prior to laser excitation, of each population, free TAHz, 1:1 complex, and 1:2 complex to be 4.3, 2.8, and 0.4 μ M, respectively. These results indicate that in our emission measurements, we are primarily monitoring emission from the free and 1:1 complexes. Indeed, using time-resolved photoluminescence (TR-PL) and global analysis, we extract only two distinct spectral components, described in detail previously.¹⁷ Briefly, temporally and spectrally resolved photoluminescence data are collected using a streak camera for solutions of TAHz in the presence of 100 mM phenol. These three-dimensional data sets are analyzed using global analysis, which allows us to kinetically resolve overlapping spectral features.³⁸ We model the time- and wavelengthdependent PL intensity $\Theta(t,\lambda)$ at time t and wavelength λ as a sum of concentration-weighted spectral components such that $\Theta(t,\lambda) = \sum_{i} c_i(t) \sigma_i(\lambda)$, where $c_i(t)$ and $\sigma_i(\lambda)$, respectively, correspond to the time-dependent concentration and wavelength-dependent species-associated emission spectrum (SAES) of the *i*th emissive species.³⁸ Global analysis yields two kinetically resolvable emission features, shown in Figure 3A, with kinetics shown in Figure 3B. We attribute the spectral feature at lower energies to free TAHz chromophores, the lifetime of which follows Stern-Volmer kinetics with changing

phenol concentration, suggesting collisional quenching. The spectral feature at higher energies corresponds to the faster decay rate and is attributed to the TAHz-PhOH complex (see Section SIII). A complete discussion regarding the nature of these spectral features can be found in our previous publication.¹⁷

When we compare the fast-component emission spectra, shown in Figure 3C, we notice significant spectral changes across the phenol series, yet the slow component emission spectra, Figure 3D, remain nearly identical. Initially, we considered whether this effect could be due to an increase in the dielectric constant of the solution due to the increasingly polar phenol. However, the emission spectra of TAHz in toluene ($\varepsilon \sim 2.4$) appears to be identical to the spectral shape in a 50:50 toluene:benzonitrile mixture ($\varepsilon_{
m benzonitrile} \sim 26$), shown in Figure S4, despite an increase in the solvent dielectric constant of more than an order of magnitude. Upon further inspection, it appears that spacing between vibronic peaks remains more or less unchanged among all fast and slow component spectra, which suggests that the vibronic progression in all spectra likely reports on the TAHz-centered vibrational modes with the same vibrational character. Rather, what is changing is the relative intensity of the peaks, or the Franck-Condon progression. This redistribution of oscillator strength between the vibronic peaks suggests varying degrees of nuclear displacement in the excited state along a representative vibrational coordinate; less displacement is observed in complexes with higher Hammett parameters and more displacement is observed for lower Hammett parameters. Initially, it was quite surprising to observe that a pendant group on phenol could influence the excited-state displacement of a local TAHz vibration. However, this somewhat unintuitive result highlights how the hydrogen bond can alter the broader excited-state landscape. A deeper understanding of this picture could provide opportunities for rationally designed hydrogen-bonding environments or controlling reactions by specifically exciting molecular vibrations on the chromophore. In order to quantitatively analyze these spectral changes, in the next section, we will turn to a displaced-oscillator model of molecular emission.

Modeling the Emission Lineshape. Analysis of absorption and emission lineshapes has helped reveal photophysics of organic molecules for decades.³⁹ For example, the vibronic structure observed in benzophenone corresponds to the C=O stretching (~1700 cm⁻¹), which allows for the mixing of the $\pi\pi^*$ character into the otherwise forbidden $n\pi^*$ transition. There exists a vast body of literature focused on understanding the vibronic coupling in optoelectronic materials to guide materials design for applications such as organic solar cells and light emitting dioides.^{8,40-43} It is common to quantify molecular distortion in the excited state by the Huang-Rhys (HR) factor, which is a unitless measure of the electronvibration coupling strength and is also directly related to the relative displacement of the nuclear coordinate in the Franck-Condon picture. 40,41,43 This is typically achieved by fitting Gaussian curves to the spectra and using their areas or peak heights to assume HR = $I_{1\leftarrow 0}/I_{0\leftarrow 0}$, where $I_{1\leftarrow 0}$ is the intensity of the transition from the zeroth vibrational state in the first electronic state to the first vibrational state in the ground electronic state and $I_{0\leftarrow 0}$ is the intensity of the transition from the zeroth vibrational state in the first electronic state to the zeroth vibrational state in the ground electronic state. A large HR factor is calculated for spectra with small oscillator strength of the $0 \rightarrow 0$ and represents significant excited-state displacement along a certain vibrational coordinate.

However, when Gaussians were fit to the spectral traces, as shown in Figure S5, the individual Gaussian curves were of varying widths and nonuniform spacing. This alone calls into question the underlying assumption that a single vibrational mode is coupled to the electronic transition, but we also found that the HR factors predicted by our Gaussian fits were often over 4 (see Section SIV). This prediction is contradictory to literature precedent for how a high HR vibronic progression should appear. 43 Evidently, in our case, this approach does not adequately capture all relevant physics needed to describe the system. As such, we surmised that more than one vibrational mode could be coupled to the electronic transition and contribute to the observed spectra. Therefore, to best understand how changing the R-group on the phenol influences multiple modes of molecular distortion in the excited state, we implemented a model of vibronic emission to fit the spectra. Within the displaced-oscillator model, a chosen number of vibrational modes are represented by harmonic oscillators whose equilibrium position becomes displaced upon excitation of the adiabatically coupled electronic transition, pictorially depicted in Figure 4A; for the interested reader, see Sections SIV and SVI for the derivation and instructions for finding the publicly available code.³¹ By least-squares fitting this model (with two vibrational modes) to the data, we extract six physically meaningful parameters: the $0 \rightarrow 0$ transition energy (E_{00}) , the frequency of each vibrational mode (ω_1) and ω_2), the displacement of each mode upon excitation in terms of unitless HR factors (HR1 and HR2), and a damping coefficient (γ) which broadens the individual vibronic peaks and is attributed to non-hydrogen-bonding interactions with

the solvent. In this context, the HR factor is directly related to the equilibrium displacement d_i of the electronic potential along the nuclear vibration coordinate. For the i^{th} vibrational mode, the HR factor is $\text{HR}_i = \frac{d_i^2}{2} \frac{m_i \omega_i}{\hbar}$, where the displacement squared is rendered dimensionless by the oscillator effective mass m_i , the vibrational frequency ω_i , and the reduced Planck constant \hbar . While this factor was originally used in ionic crystals, it has since been applied more broadly and allows us to quantitatively compare molecular displacement upon emission.⁴⁴

Figure 4B shows the area-normalized model fit to the fast component extracted from the TAHz-PhOH TR-PL data set. With two vibrational modes, the model appears to fit the data well and does not significantly improve upon the addition of a third mode (both R² values are 0.965). The area-normalized contribution from each mode is shown in the bottom plot of Figure 4B. We extract two modes: a high-frequency mode at 1070 cm⁻¹ and a low-frequency mode at 185 cm⁻¹. To gain physical insights into what vibrational modes these transitions represent, we turn to quantum chemical calculations (Section Quantum Chemical Calculations).

Fitting the extracted fast-component spectra with this model allows us to quantify the displacement of each mode across the series of complexes for all R-groups of the phenols, as shown in Figure 5A. The extracted frequencies and HR factors for each TAHz-R-PhOH complex are displayed in Table 1. Most notably, we see a clear trend of the decreasing HR factor (proportional to the displacement squared) with the increasing

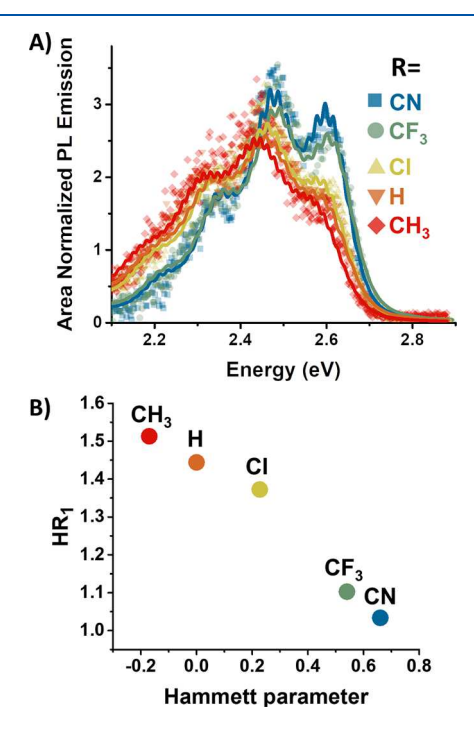


Figure 5. (A) Data (dots) compared to displaced-oscillator model fit (solid lines) for all phenol derivatives. Fits for each spectrum are shown individually in Figures S7–S11. (B) HR parameter for the high-frequency mode as a function of the Hammett parameter of the para-substituent on phenol; values are shown in Table 1. We observe that greater molecular distortion appears to correlate with weaker hydrogen bonds (lower Hammett parameters). From these data, we note that the stronger the hydrogen bond, the less distorted the molecule becomes in the excited state.

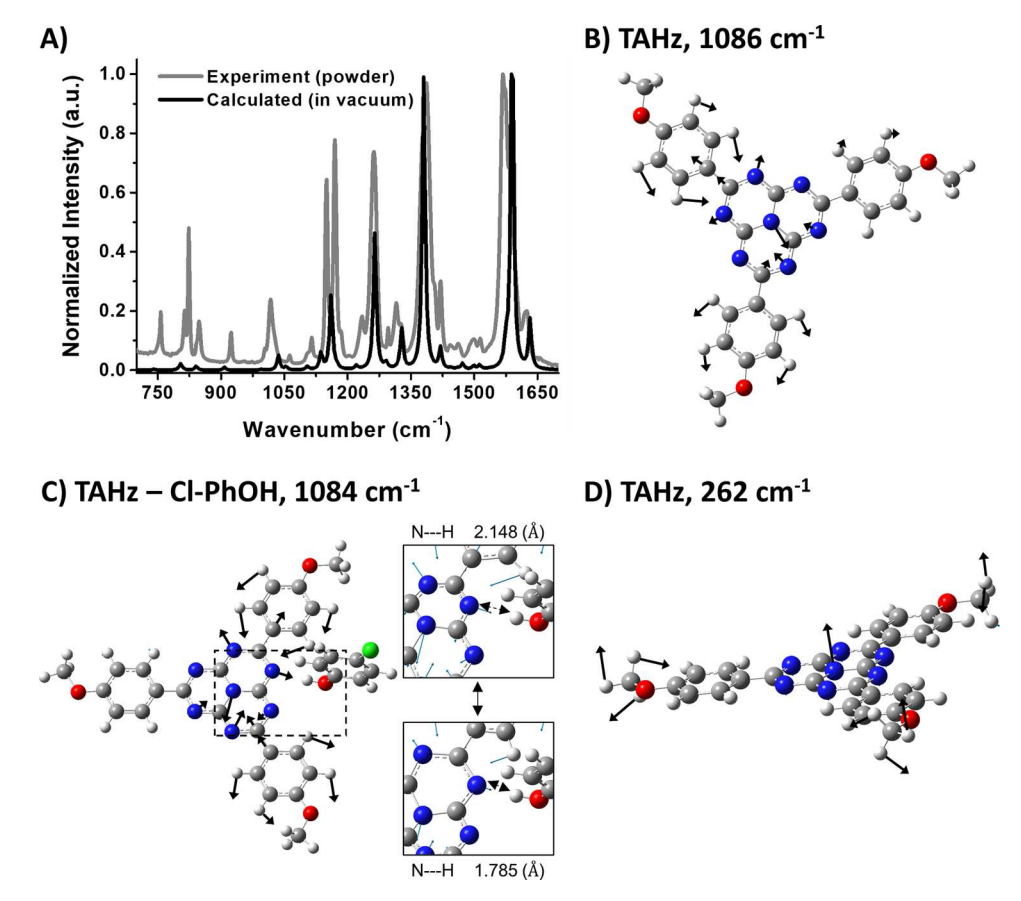


Figure 6. (A) FTIR spectrum of TAHz powder (gray) compared to the calculated FTIR spectrum in vacuum (back). The range of transitions in the 1000–1600 cm⁻¹ range displayed in Table 1 are generally attributed to heptazine ring-breathing and C–N stretching modes. (B) Example molecular vibration calculated to be 1086 cm⁻¹ is shown by the displacement vectors; see the Supporting Information for more images. The high-frequency mode extracted from the PL spectral fit is attributed to one of these modes which is modulated by the nearby PhOH. (C) Example heptazine ring-breathing vibration of TAHzCl–PhOH complex that modulate N–H hydrogen bonding distance significantly. (D) Low-frequency mode around 262 cm⁻¹ corresponds to the ring-puckering, wherein the central nitrogen moves up out of plane, and the outer nitrogens move down; see Supporting Information for more images.

electron-withdrawing effect for the high-frequency mode. The nearly linear correlation between the HR factor and Hammett parameter for the high-frequency mode is shown in Figure 5B. We also observe that the distortion decreases for the lowfrequency mode with the increasing Hammett parameter; see Section SIV. However, we acknowledge that thermal energy at room temperature is on the order of 200 cm⁻¹. Additionally, the covariance matrices returned by the least-squares fits indicate moderate correlation between the damping coefficient and the low-frequency mode parameters. This result may be expected, considering that the low-frequency vibronic progression effectively broadens the more distinct high-frequency peaks upon convolution of the independent mode emission spectra shown in Figure 4B. Therefore, despite needing the low-frequency mode to accurately describe the spectra, we take some caution in interpreting the numerical quantities assigned to the low-frequency mode.

Our computational results suggest that the hydrogen-bonding interaction in the R-PhOH-TAHz complexes results in significant symmetry breaking that imparts oscillator strength (Figure S13) to the otherwise forbidden S_1 transition. As such, the Franck–Condon approximation is evidentially sufficient to adequately capture the spectral shape. We note that neither the slow TAHz emission component nor the free TAHz spectral shapes could be adequately captured by the

harmonic oscillator model, as shown in Figure S12. Possible reasons for this may include anharmonicity of the potential surface (see Section SIV), a greater relative importance of nonadiabatic intensity borrowing from an allowed state, and the symmetry-forbidden nature of the transition resulting in a greater relative importance of Herzberg—Teller effects. However, it is interesting to recall that the spectral shape associated with non-hydrogen-bonded species, both from the slow component and free TAHz emission spectrum, show a greater molecular displacement in the excited state than any of the fast-component spectra. Therefore, it appears that the hydrogen bond hinders molecular distortion of the heptazine chromophore in the excited state.

Quantum Chemical Calculations. To help visualize the molecular vibrations, we used DFT and TD-DFT calculations; see Section SV of the Supporting Information. Using the optimized ground-state geometry of TAHz, we calculated the normal modes and FTIR spectrum shown in Figure 6A. The calculated spectrum shows surprisingly good agreement with the experimental FTIR of TAHz powder. There exist a number of vibrational transitions in the 1000–1200 cm⁻¹ region that are generally attributable to heptazine ring-breathing modes and C–N stretching. An example of such a vibration is shown in Figure 6B, wherein the center nitrogen is displaced off-axis within the heptazine plane, with two of the peripheral

nitrogens within the heptazine ring being displaced outwardly in the opposite directions. Figure S16 shows other ringbreathing vibrations in the 1000-1200 cm⁻¹ frequency range. Animations to visualize these nuclear motions are provided with the Supporting Information. It is conceivable that these ring-breathing modes could be strongly coupled to the electronic transition; the symmetry-forbidden $\pi\pi^*$ S₁ transition must couple to vibrations which break the symmetry of the heptazine ring. In light of these results, the vibrational distortion of the chromophore in the excited state appears to be influenced by the hydrogen-bonding interaction of the peripheral nitrogen to the phenol species. The modulation of the N-H hydrogen bond distance could possibly even serve as a handle for reactivity. Preliminary results from DFT calculation of the TAHz-Cl-PhOH complex showed that the N-H hydrogen bond distance can be significantly modulated by heptazine ring-breathing vibrations (Figure 6C and Figures S17,S18), both at ground-state and symmetry-forbidden $\pi\pi^*$ excited-state optimized geometry.

While the low-frequency mode is outside the experimental window in Figure 6, quantum chemical calculations for heptazine predict that the ring puckers out of plane in the excited state and the inversion of this umbrella motion occurs in the 200-300 cm⁻¹ range, as shown in Figure 6D and Figure S14. This puckering not only breaks the planarity of the heptazine chromophore, but also imparts a double-well character on the potential energy surface of the excited state. It should be noted that the displaced-oscillator model of molecular emission does not allow for specific mode assignment beyond matching the resonance frequency. It is therefore possible that the vibrational modes predicted by the model more accurately represent a collection of modes closely spaced in energy. In this case, the predicted HR parameter would be approximately the sum of those HR parameters from each contributing mode, and the predicted frequency would be a weighted average of contributing modes.⁴⁹ We expect that this, along with the correlation in predicted parameters with the damping coefficient (discussed above), is the likely cause of the numerical discrepancy between low-energy mode frequency predicted by the displaced-oscillator emission model and the quantum chemical calculations.

CONCLUSIONS

Using a series of phenol derivatives, we modulate the electronwithdrawing nature of the hydrogen bond donor and systematically study the hydrogen-bonding interactions with a heptazine chromophore. We observe stronger hydrogen bonds for larger Hammett parameters, as expected. By kinetically resolving and comparing individual PL spectral components for this series of hydrogen-bonded complexes, we see a trend of decreasing displacement of the S₁ and S₀ equilibrium geometries with increasing intermolecular hydrogen bond strength. By implementing a displaced-oscillator model to fit the PL spectral components, we extract the frequencies and displacements of two vibrational modes that are most strongly coupled to the S₁ electronic transition. We use this information to monitor how these coupling strengths are influenced by varying hydrogen bond strength. From quantum chemical calculations, we further visualize pertinent TAHz-centered molecular vibrations, which correspond to heptazine ring-breathing modes around 1100 cm⁻¹ and umbrella-like modes involving an out-of-plane puckering of the central nitrogen atom near 200 cm⁻¹.

Altering the extent of distortion along each of these modes has interesting implications for ES-PCET and ES-PT reactions, as they both modulate the position of the hydrogen-bonded nitrogen. As we previously showed, the out-of-plane puckering in the excited state breaks the symmetry of the heptazine core and increases the oscillator strength of transitions to higherlying excited states, thus enabling further optical control of the photochemical reactivity of these complexes using ultrafast spectroscopy.³⁰

Additionally, this new insight may help inform molecular design parameters to enable future advanced materials discovery for solar energy conversion and storage. Seeing how the stronger hydrogen-bonded complexes undergo less distortion of the heptazine ring in the excited state, it is interesting to return to the reactivity difference of H-PhOH and Cl-PhOH. Given the same driving force for electron transfer, it is possible that the excited-state molecular distortion may have the effect of hindering the ES-PCET reaction. While adding electron-withdrawing groups to heptazine could increase the ES-PCET reactivity, we have found here that it is also important to consider tailoring the hydrogen-bonding environment. In particular, if one aims to increase ES-PCET with water, our results suggest that tailored hydrogen bonding environments may provide a critical molecular design parameter moving forward. Work is ongoing in our lab to control both the oxidation potential and the hydrogen-bonding environment around the heptazine core through chemical functionalization of the chromophore. Additionally, we are working to implement an anharmonic extension to the displaced-oscillator model, which could provide insights into the unbound TAHz emission. We anticipate that this work will provide a more comprehensive picture of the excited-state landscape and how it can be altered by hydrogen bonding and chromophore design.

ASSOCIATED CONTENT

Supporting Information

The Supporting Information is available free of charge at https://pubs.acs.org/doi/10.1021/acs.jpcb.0c07719.

Materials and methods, $K_{\rm A}$ determination, time-resolved photoluminescence spectra for the phenol series, spectral model details, additional quantum chemical calculation results, and a full derivation (PDF)

Movie S1: animations of TAHz ring puckering vibrational modes (AVI)

Movie S2: animations of TAHz ring breathing vibrational modes (AVI)

Movie S3: animations of a [TAHz-Cl-PhOH] ring breathing vibrational mode in the ground- and excited-state (AVI)

Movie S4: animations of a [TAHz–Cl-PhOH] ring breathing vibrational mode in ground- and excited-state (AVI)

AUTHOR INFORMATION

Corresponding Author

Cody W. Schlenker – Department of Chemistry, University of Washington, Seattle, Washington 98195, United States; Molecular Engineering and Sciences Institute and Clean Energy Institute, University of Washington, Seattle, Washington 98195-1652, United States; orcid.org/0000-0003-3103-402X; Email: schlenk@uw.edu

Authors

- Emily J. Rabe Department of Chemistry, University of Washington, Seattle, Washington 98195, United States; orcid.org/0000-0002-9397-049X
- Harrison J. Goldwyn Department of Chemistry, University of Washington, Seattle, Washington 98195, United States; orcid.org/0000-0002-7184-2120
- Doyk Hwang Department of Chemistry, University of Washington, Seattle, Washington 98195, United States; orcid.org/0000-0001-5275-0354
- David J. Masiello Department of Chemistry, University of Washington, Seattle, Washington 98195, United States;
 orcid.org/0000-0002-1187-0920

Complete contact information is available at: https://pubs.acs.org/10.1021/acs.jpcb.0c07719

Author Contributions

*E.J.R. and H.J.G. contributed equally. The manuscript was written through contributions of all authors. All authors have given approval to the final version of the manuscript.

Notes

The authors declare no competing financial interest.

ACKNOWLEDGMENTS

We are grateful to Professor Wolfgang Domcke, Xiang Huang, and Professor Andrzej Sobolewski for their helpful discussions and input regarding this work. This work is based on research that was supported in part by the Washington Research Foundation and the University of Washington Clean Energy Institute (CEI). Part of this work was conducted at the Molecular Analysis Facility, a National Nanotechnology Coordinated Infrastructure (NNCI) site at the University of Washington, which is supported in part by funds from the National Science Foundation (awards NNCI-2025489, NNCI-1542101), the Molecular Engineering & Sciences Institute, and the Clean Energy Institute. C. W. S. acknowledges that a portion of this material is based upon work supported by the US National Science Foundation (NSF) under Grant No. [1846480]. H.J.G and D.J.M acknowledge that the modeling of the emitter's photophysics was supported by NSF Grant CHE-1727092. DFT and TD-DFT calculations were facilitated through the use of advanced computational, storage, and networking infrastructure provided by the Hyak supercomputer system and funded by the STF at the University of Washington.

REFERENCES

- (1) Tommos, C.; Babcock, G. T. Proton and Hydrogen Currents in Photosynthetic Water Oxidation. *Biochem. Biophys. Acta* **2000**, *1458*, 199–219.
- (2) Warren, J. J.; Tronic, T. A.; Mayer, J. M. Thermochemistry of Proton-Coupled Electron Transfer Reagents and its Implications. *Chem. Rev.* **2010**, *110*, 6961–7001.
- (3) Crivello, J. V. The Discovery and Development of Onium Salt Cationic Photoinitiators. *J. Polym. Sci., Part A: Polym. Chem.* **1999**, 37, 4241–4254.
- (4) Roy, S.; Ardo, S.; Furche, F. 5-Methoxyquinoline Photobasicity Is Mediated by Water Oxidation. *J. Phys. Chem. A* **2019**, *123*, 6645–6651
- (5) Kwon, J. E.; Park, S. Y. Advanced Organic Optoelectronic Materials: Harnessing Excited-State Intramolecular Proton Transfer (ESIPT) Process. *Adv. Mater.* **2011**, *23*, 3615–3642.

- (6) Padalkar, V. S.; Seki, S. Excited-State Intramolecular Proton-Transfer (ESIPT)-Inspired Solid State Emitters. *Chem. Soc. Rev.* **2016**, 45, 169–202.
- (7) Harshan, A. K.; Yu, T.; Soudackov, A. V.; Hammes-Schiffer, S. Dependence of Vibronic Coupling on Molecular Geometry and Environment: Bridging Hydrogen Atom Transfer and Electron—Proton Transfer. *J. Am. Chem. Soc.* **2015**, *137*, 13545–13555.
- (8) Hestand, N. J.; Spano, F. C. Expanded Theory of H- and J-Molecular Aggregates: The Effects of Vibronic Coupling and Intermolecular Charge Transfer. *Chem. Rev.* **2018**, *118*, 7069–7163.
- (9) Han, F.; Liu, W.; Zhu, L.; Wang, Y.; Fang, C. Initial Hydrogen-Bonding Dynamics of Photoexcited Coumarin in Solution with Femtosecond Stimulated Raman Spectroscopy. *J. Mat. Chem. C* **2016**, 4, 2954–2963.
- (10) Zhao, G.-J.; Han, K.-L. Early Time Hydrogen-Bonding Dynamics of Photoexcited Coumarin 102 in Hydrogen-Donating Solvents: Theoretical Study. *J. Phys. Chem. A* **2007**, *111*, 2469–2474.
- (11) Barman, N.; Singha, D.; Sahu, K. Fluorescence Quenching of Hydrogen-Bonded Coumarin 102-Phenol Complex: Effect of Excited-State Hydrogen Bonding Strength. *J. Phys. Chem. A* **2013**, *117*, 3945–3953
- (12) Hunt, J. R.; Dawlaty, J. M. Kinetic Evidence for the Necessity of Two Proton Donor Molecules for Successful Excited State Proton Transfer by a Photobase. *J. Phys. Chem. A* **2019**, *123*, 10372–10380.
- (13) Dongare, P.; Bonn, A. G.; Maji, S.; Hammarström, L. Analysis of Hydrogen-Bonding Effects on Excited-State Proton-Coupled Electron Transfer from a Series of Phenols to a Re(I) Polypyridyl Complex. J. Phys. Chem. C 2017, 121, 12569–12576.
- (14) Demeter, A.; Ravasz, L.; Bérces, T. Influence of Hydrogen Bond Formation on the Photophysics of N-(2,6-Dimethylphenyl)-2,3-naphthalimide. *J. Phys. Chem. A* **2004**, *108*, 4357–4364.
- (15) Ehrmaier, J.; Karsili, T. N. V.; Sobolewski, A. L.; Domcke, W. Mechanism of Photocatalytic Water Splitting with Graphitic Carbon Nitride: Photochemistry of the Heptazine-Water Complex. *J. Phys. Chem. A* **2017**, *121*, 4754–4764.
- (16) Liu, X.; Karsili, T. N.; Sobolewski, A. L.; Domcke, W. Photocatalytic Water Splitting with the Acridine Chromophore: A Computational Study. *J. Phys. Chem. B* **2015**, *119*, 10664–10672.
- (17) Rabe, E. J.; Corp, K. L.; Huang, X.; Ehrmaier, J.; Flores, R. G.; Estes, S. L.; Sobolewski, A. L.; Domcke, W.; Schlenker, C. W. Barrierless Heptazine-Driven Excited State Proton-Coupled Electron Transfer: Implications for Controlling Photochemistry of Carbon Nitrides and Aza-Arenes. J. Phys. Chem. C 2019, 123, 29580–29588.
- (18) Balasubramanian, M.; Reynolds, A.; Blair, T. J.; Khalil, M. Probing Ultrafast Vibrational Dynamics of Intramolecular Hydrogen Bonds with Broadband Infrared Pump-probe Spectroscopy. *Chem. Phys.* **2019**, *519*, 38–44.
- (19) Schriever, C.; Barbatti, M.; Stock, K.; Aquino, A. J. A.; Tunega, D.; Lochbrunner, S.; Riedle, E.; de Vivie-Riedle, R.; Lischka, H. The Interplay of Skeletal Deformations and Ultrafast Excited-State Intramolecular Proton Transfer: Experimental and Theoretical Investigation of 10-hydroxybenzo[h]quinoline. *Chem. Phys.* **2008**, 347, 446–461.
- (20) Fujisawa, T.; Kuramochi, H.; Hosoi, H.; Takeuchi, S.; Tahara, T. Role of Coherent Low-Frequency Motion in Excited-State Proton Transfer of Green Fluorescent Protein Studied by Time-Resolved Impulsive Stimulated Raman Spectroscopy. *J. Am. Chem. Soc.* **2016**, 138, 3942–3945.
- (21) Fang, C.; Frontiera, R. R.; Tran, R.; Mathies, R. A. Mapping GFP Structure Evolution During Proton Transfer with Femtosecond Raman Spectroscopy. *Nature* **2009**, *462*, 200–204.
- (22) Zhang, G.; Lin, L.; Li, G.; Zhang, Y.; Savateev, A.; Zafeiratos, S.; Wang, X.; Antonietti, M. Ionothermal Synthesis of Triazine—Heptazine-Based Copolymers with Apparent Quantum Yields of 60% at 420 nm for Solar Hydrogen Production from "Sea Water". *Angew. Chem., Int. Ed.* **2018**, *57*, 9372–9376.
- (23) Lau Vincent, W. H.; Klose, D.; Kasap, H.; Podjaski, F.; Pignié, M. C.; Reisner, E.; Jeschke, G.; Lotsch Bettina, V. Dark Photo-

- catalysis: Storage of Solar Energy in Carbon Nitride for Time-Delayed Hydrogen Generation. *Angew. Chem., Int. Ed.* **2017**, *56*, 510–514.
- (24) Markushyna, Y.; Lamagni, P.; Teutloff, C.; Catalano, J.; Lock, N.; Zhang, G.; Antonietti, M.; Savateev, A. Green Radicals of Potassium Poly(heptazine imide) Using Light and Benzylamine. *J. Mat. Chem. A* **2019**, *7*, 24771–24775.
- (25) Yan, S. C.; Li, Z. S.; Zou, Z. G. Photodegradation of Rhodamine B and Methyl Orange over Boron-Doped g-C3N4 under Visible Light Irradiation. *Langmuir* **2010**, *26*, 3894–3901.
- (26) Ong, W. J.; Tan, L. L.; Ng, Y. H.; Yong, S. T.; Chai, S. P. Graphitic Carbon Nitride (g-C3N4)-Based Photocatalysts for Artificial Photosynthesis and Environmental Remediation: Are We a Step Closer To Achieving Sustainability? *Chem. Rev.* **2016**, *116*, 7159–7329.
- (27) Lau, V. W.; Moudrakovski, I.; Botari, T.; Weinberger, S.; Mesch, M. B.; Duppel, V.; Senker, J.; Blum, V.; Lotsch, B. V. Rational Design of Carbon Nitride Photocatalysts by Identification of Cyanamide Defects as Catalytically Relevant Sites. *Nat. Commun.* **2016**, *7*, 12165.
- (28) Ullah, N.; Chen, S.; Zhao, Y.; Zhang, R. Photoinduced Water—Heptazine Electron-Driven Proton Transfer: Perspective for Water Splitting with g-C3N4. J. Phys. Chem. Lett. 2019, 10, 4310–4316.
- (29) Rabe, E. J.; Corp, K. L.; Sobolewski, A. L.; Domcke, W.; Schlenker, C. W. Proton-Coupled Electron Transfer from Water to a Model Heptazine-Based Molecular Photocatalyst. *J. Phys. Chem. Lett.* **2018**, *9*, 6257–6261.
- (30) Corp, K. L.; Rabe, E. J.; Huang, X.; Ehrmaier, J.; Kaiser, M. E.; Sobolewski, A. L.; Domcke, W.; Schlenker, C. W. Control of Excited-State Proton-Coupled Electron Transfer by Ultrafast Pump-Push-Probe Spectroscopy in Heptazine-Phenol Complexes: Implications for Photochemical Water Oxidation. *J. Phys. Chem. C* **2020**, 9151.
- (31) Mukamel, S., Principles of Nonlinear Optical Spectroscopy. Oxford University Press: 1995.
- (32) Frisch, M. J.; Trucks, G. W.; Schlegel, H. B.; Scuseria, G. E.; Robb, M. A.; Cheeseman, J. R.; Scalmani, G.; Barone, V.; Petersson, G. A.; Nakatsuji, H.; et al. *Gaussian 16 Rev. C.01*, Wallingford, CT, 2016.
- (33) Bronner, C.; Wenger, O. S. Kinetic Isotope Effects in Reductive Excited-State Quenching of Ru(2,2'-bipyrazine)32+ by Phenols. *J. Phys. Chem. Lett.* **2011**, 3, 70–74.
- (34) Bronner, C.; Wenger, O. S. Proton-Coupled Electron Transfer between 4-Cyanophenol and Photoexcited Rhenium(I) Complexes with Different Protonatable Sites. *Inorg. Chem.* **2012**, *51*, 8275–8283.
- (35) Hansch, C.; Leo, A.; Taft, R. W. A Survey of Hammett Substituent Constants and Resonance and Field Parameters. *Chem. Rev.* 1991, 91, 165–195.
- (36) Demeter, A.; Mile, V.; Bérces, T. Hydrogen Bond Formation between 4-(Dimethylamino)pyridine and Aliphatic Alcohols. *J. Phys. Chem. A* **2007**, *111*, 8942–8949.
- (37) Ehrmaier, J.; Rabe, E. J.; Pristash, S. R.; Corp, K. L.; Schlenker, C. W.; Sobolewski, A. L.; Domcke, W. Singlet—Triplet Inversion in Heptazine and in Polymeric Carbon Nitrides. *J. Phys. Chem. A* **2019**, 123, 8099—8108.
- (38) Snellenburg, J. J.; Laptenok, S. P.; Seger, R.; Mullen, K. M.; Stokkum, I. H. M. V. Glotaran: A Java-Based Graphical User Interface for the R Package TIMP. *J. Stat. Softw.* **2012**, *49*, 22.
- (39) Turro, N. J.; Ramamurthy, V.; Scaiano, J. C., Principles of Molecular Photochemistry: An Introduction. University Science Books Sausalito, California, 2009.
- (40) Lim, S.-H.; Bjorklund, T. G.; Bardeen, C. J. Temperature-Dependent Exciton Dynamics in Poly(p-phenylene vinylene) Measured by Femtosecond Transient Spectroscopy. *Chem. Phys. Lett.* **2001**, 342, 555–562.
- (41) Guha, S.; Rice, J. D.; Yau, Y. T.; Martin, C. M.; Chandrasekhar, M.; Chandrasekhar, H. R.; Guentner, R.; Scanduicci de Freitas, P.; Scherf, U. Temperature-Dependent Photoluminescence of Organic Semiconductors with Varying Backbone Conformation. *Phys. Rev. B* **2003**, *67*, 125204.

- (42) Cho, Y.-J.; Kim, S.-Y.; Kim, J.-H.; Crandell, D. W.; Baik, M.-H.; Lee, J.; Kim, C. H.; Son, H.-J.; Han, W.-S.; Kang, S. O. Important Role of Ancillary Ligand in the Emission Behaviours of Blue-emitting Heteroleptic Ir(iii) Complexes. *J. Mat. Chem. C* 2017, 5, 4480–4487.
- (43) de Jong, M.; Seijo, L.; Meijerink, A.; Rabouw, F. T. Resolving the Ambiguity in the Relation Between Stokes Shift and Huang—Rhys Parameter. *Phys. Chem. Chem. Phys.* **2015**, *17*, 16959—16969.
- (44) Huang, K.; Rhys, A.; Mott, N. F. Theory of Light Absorption and Non-radiative Transitions in F-centres. *Proc. R. Soc. Lond. A* **1950**, 204, 406–423.
- (45) Anda, A.; De Vico, L.; Hansen, T.; Abramavičius, D. Absorption and Fluorescence Lineshape Theory for Polynomial Potentials. *J. Chem. Theory Comput.* **2016**, *12*, 5979–5989.
- (46) Freidzon, A. Y.; Valiev, R. R.; Berezhnoy, A. A. Ab Initio Simulation of Pyrene Spectra in Water Matrices. *RSC Adv.* **2014**, *4*, 42054–42065.
- (47) D'Abramo, M.; Aschi, M.; Amadei, A. Theoretical Calculation of the Pyrene Emission Properties in Different Solvents. *Chem. Phys. Lett.* **2015**, 639, 17–22.
- (48) Miller, T. S.; Jorge, A. B.; Suter, T. M.; Sella, A.; Corà, F.; McMillan, P. F. Carbon Nitrides: Synthesis and Characterization of a New Class of Functional Materials. *Phys. Chem. Chem. Phys.* **2017**, *19*, 15613–15638.
- (49) Mustroph, H.; Towns, A. Fine Structure in Electronic Spectra of Cyanine Dyes: Are Sub-Bands Largely Determined by a Dominant Vibration or a Collection of Singly Excited Vibrations? *ChemPhysChem* **2018**, *19*, 1016–1023.